Supplementary Information

Topologically Engineered Nematic Networks with Ultrastrong Adhesion and Light-Debonding on Demand

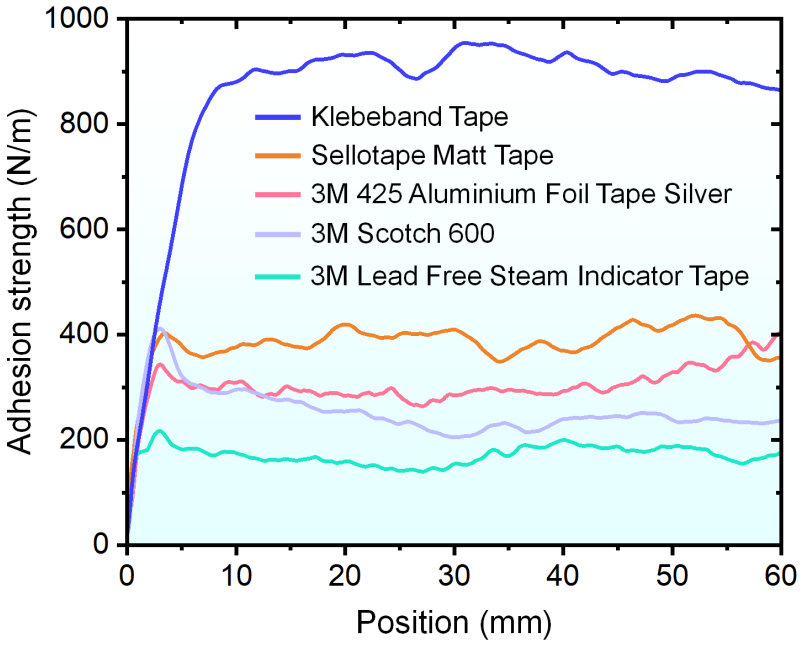

Supplementary Fig. S1. The peel strength of several commercial adhesive tapes. All the test conditions for commercial tapes are the same as those for LCE PSA.

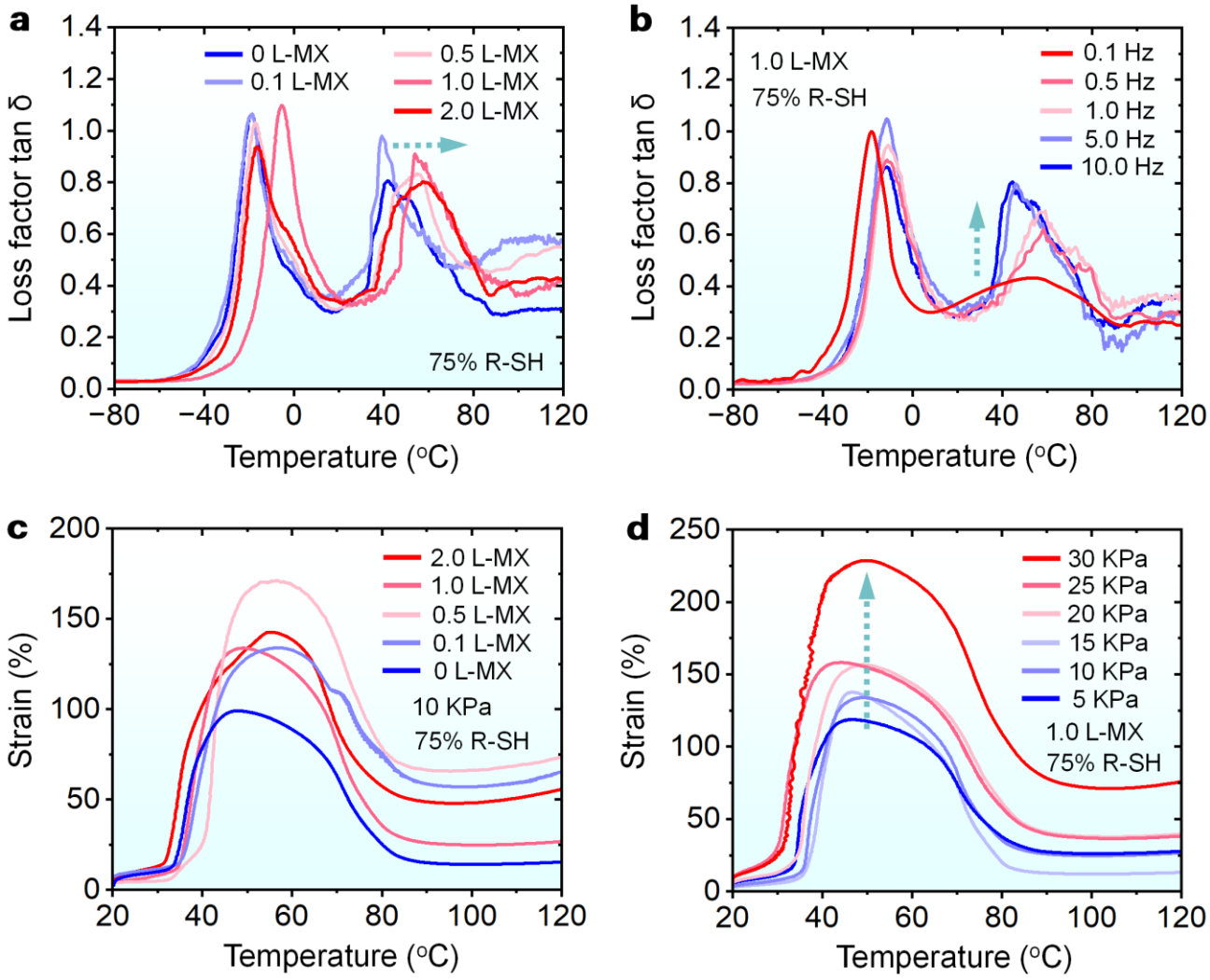

Supplementary Fig. S2. Dynamic Mechanical Analysis of LCEs. a, Loss factor tanδ of LCE with different fraction of MXene nanoplatelets, at fixed frequency of 1 Hz, on sample heating rate of 3°C/min. The increase in the MXene fraction leads to a gradual rise in the T_{ni} of LCE. This may be attributed to the fact that the presence of MXene nanoplatelets increases the energy barrier for the nematic-isotropic phase transition of the mesogens. **b**, Loss factor tanδ of 1.0 L-MX LCE at different frequency. The second-order characteristic loss factor tanδ value will increase as the frequency increases. **c**, Iso-force temperature ramp plots for LCE with different fraction of MXene, using constant engineering stress of 10 KPa and a heating rate of 3 °C/min. The embedding of MXene nanoplatelets leads to an enhancement of the creep behavior of LCE, but this effect is not monotonically related to the increase in the MXene fraction. **d**, Iso-force temperature ramp plots at different stress with a heating rate of 3 °C/min. An increase in the constant stress will lead to a significant enhancement of the LCE creep behavior.

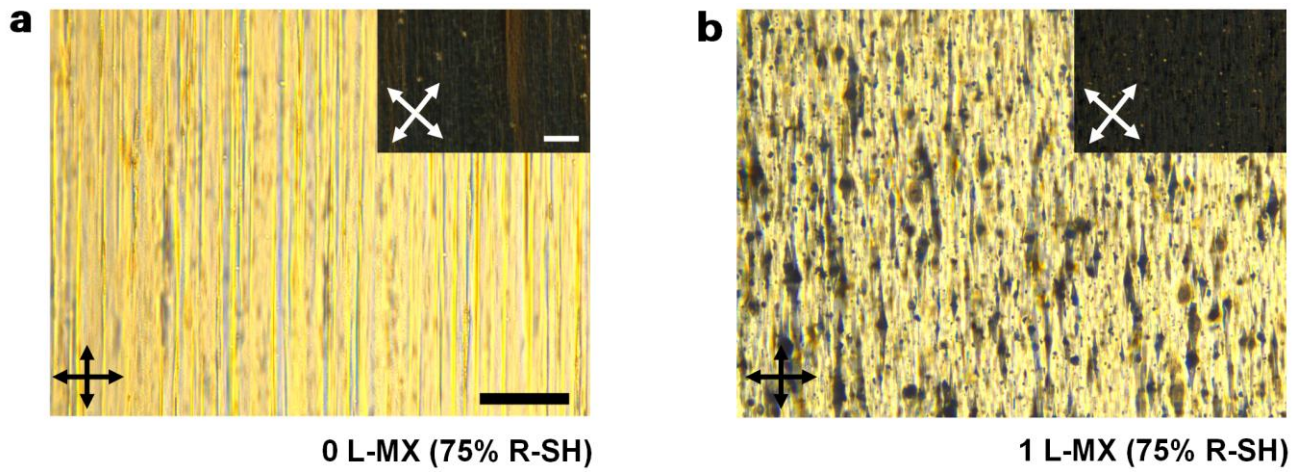

Supplementary Fig. S3. POM imgaes of pre-stretched LCEs. a, 0 L-MX. **b**, 1 L-MX. The scale bar is 100 μm. When the polarization direction rotated by 45°, the visual effect of the LCE changes from bright field to dark field, implying that the mesogens were well oriented in the film.

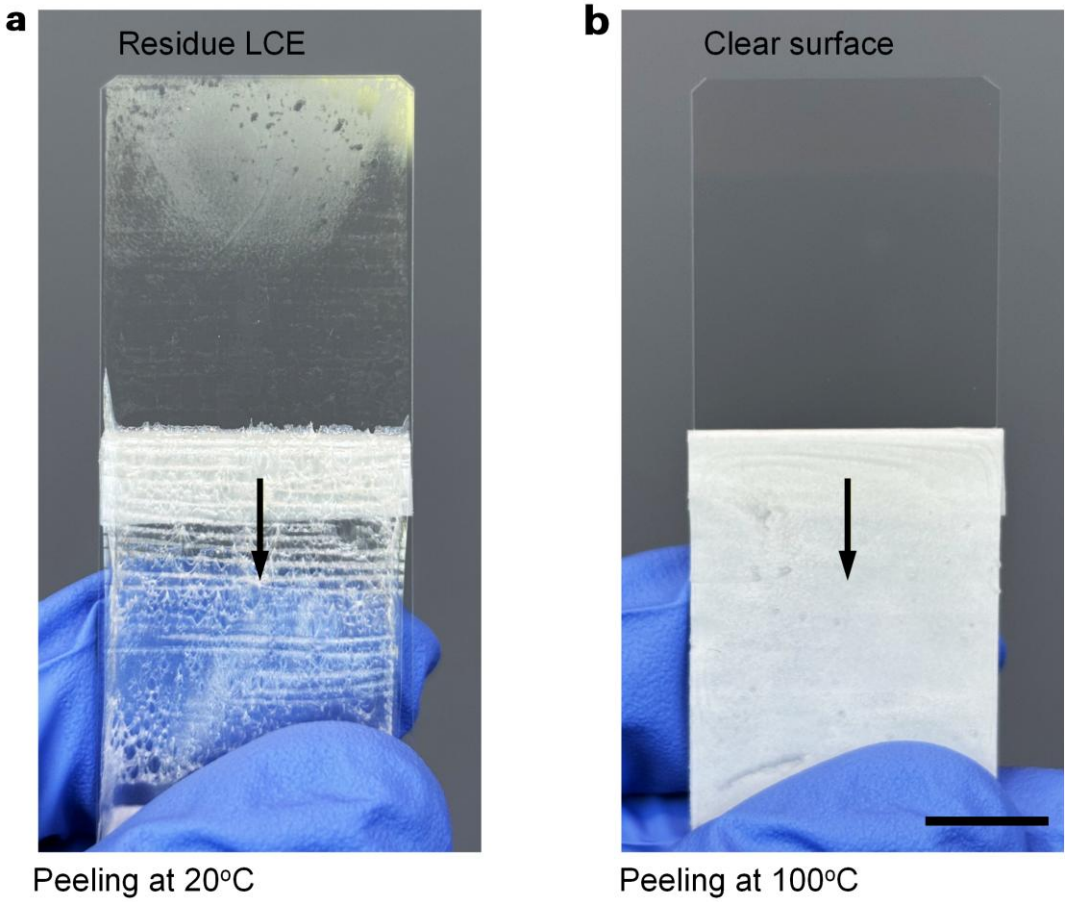

Supplementary Fig. S4. Surface state of 75% R-SH LCE after being peeled off under different conditions. a, Peeling at 20°C with a significant residue LCE on the surface. **b**, Peeling at 100°C with a clear surface. The scale bar is 10 mm.

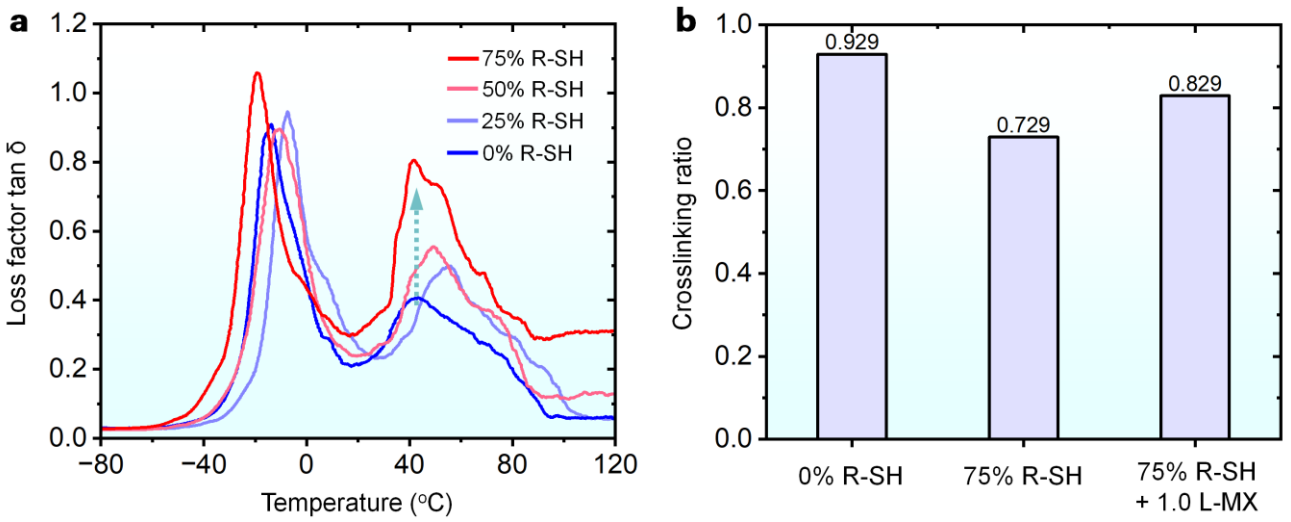

Supplementary Fig. S5. DMA temperature ramp data and crosslinking network ratio of LCE materials with dangling chains. a, Loss factor tanδ of LCE materials with different fraction of dangling chains, at fixed frequency of 1 Hz, on sample heating rate of 3°C/min. The loss factor tanδ increases monotonically with the increase of the fraction of dangling chains. **b**, Crosslinking network weight ratio of LCE. All the LCE samples were immersed in toluene for 7 days and then dried and weighted.

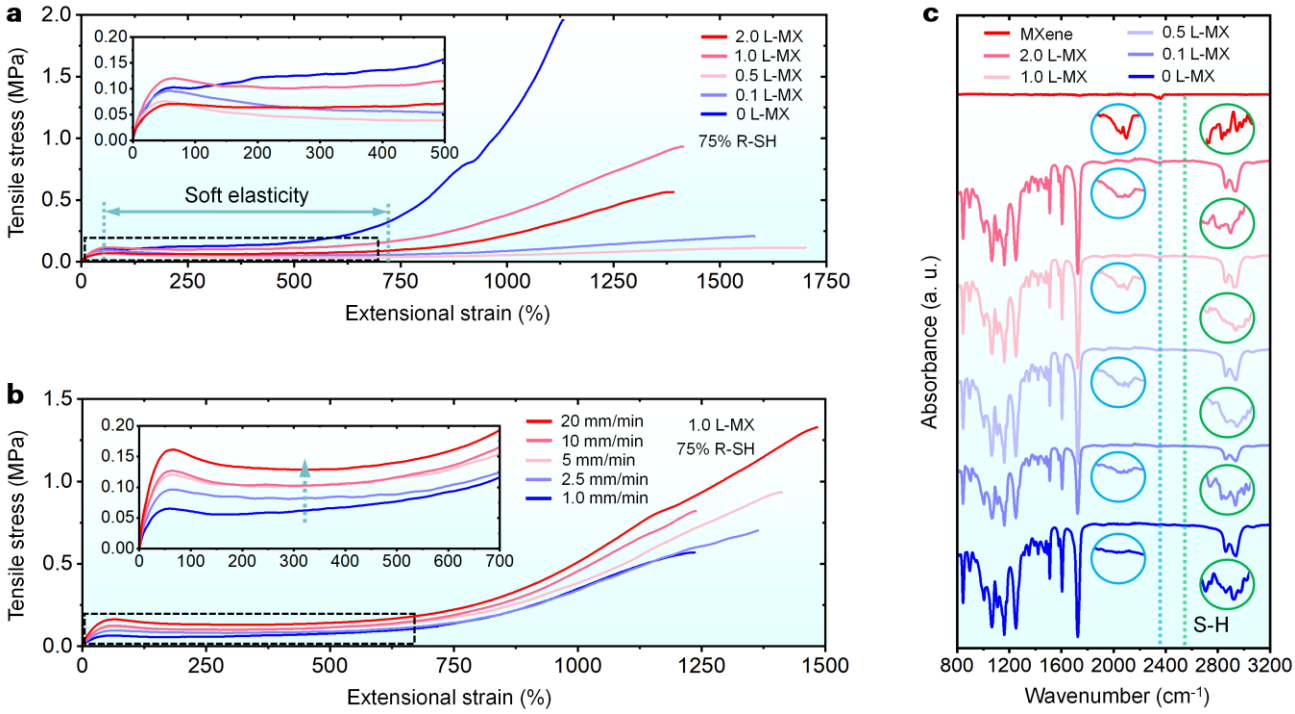

Supplementary Fig. S6. Stress-strain curves and FTIR data of LCEs. a, Stress-strain curves of 75% R-SH LCEs with different fraction of MXene nanoplatelets, at constant stretching velocity of 5 mm/min. LCEs exhibits significant soft elasticity characteristics within the strain range of approximately 100-700%. The embedding of MXene will enhance the maximum extensional strain of LCE, but this effect is not a simple monotonical relationship with the fraction of MXene. The insert is an enlarged view of the dotted frame. **b**, Stress-strain curves of LCE at different stretching velocity. Under the same strain condition, the stress of LCE monotonically increases with the increase of the stretching velocity. The insert is an enlarged view of the dotted frame. **c**, FTIR plots of LCEs and pristine MXene powder. The characteristic peaks located approximately at 2360 cm^{-1} belongs to MXene nanoplatelets. As the fraction of MXene decrease, it is obvious that the intensity of this peak gradually decreases. The characteristic peak observed at 2560 cm^{-1} originates from the vibration of -SH.

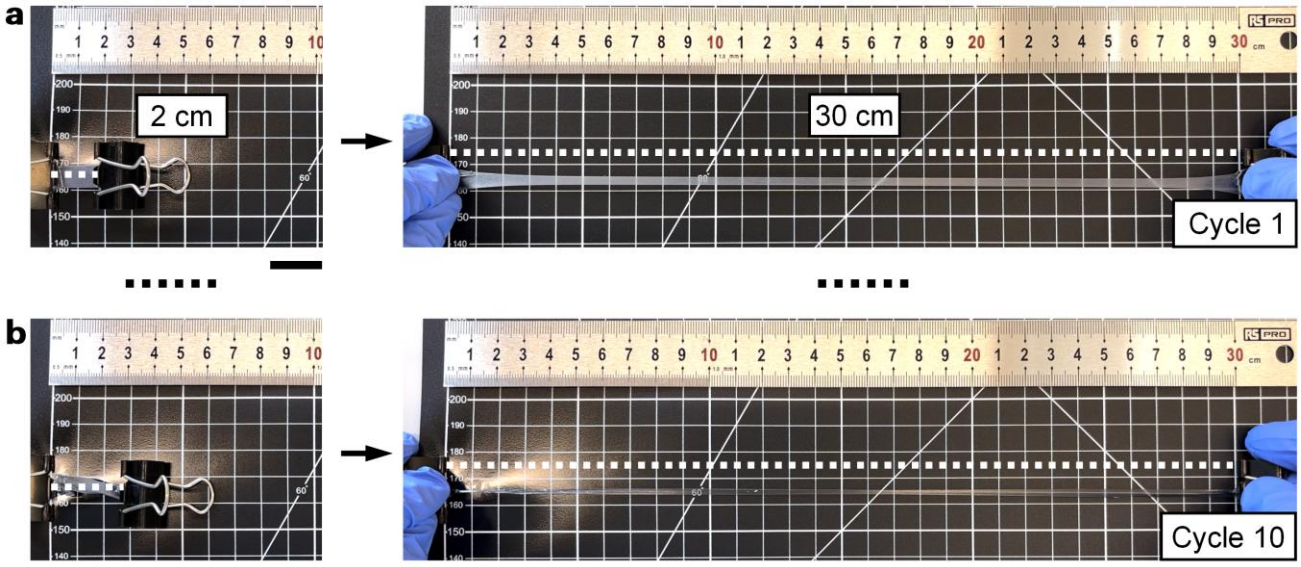

Supplementary Fig. S7. Demonstration of the excellent cyclic tensile performance of LCE (75% R-SH+1.0 wt% MXene). a, The first cycle of stretching the 2-centimer-long rectangular LCE film to a length of 30 cm. After stretching, the LCE film undergoes a nematic-isotropic phase transition upon heating and then returns to nearly its original length. **b**, The tenth cycle of stretching the 2-centimer-long rectangular LCE film to a length of 30 cm. The scale bar is 2 cm. For the complete process, please refer to Supplementary Videos 1.

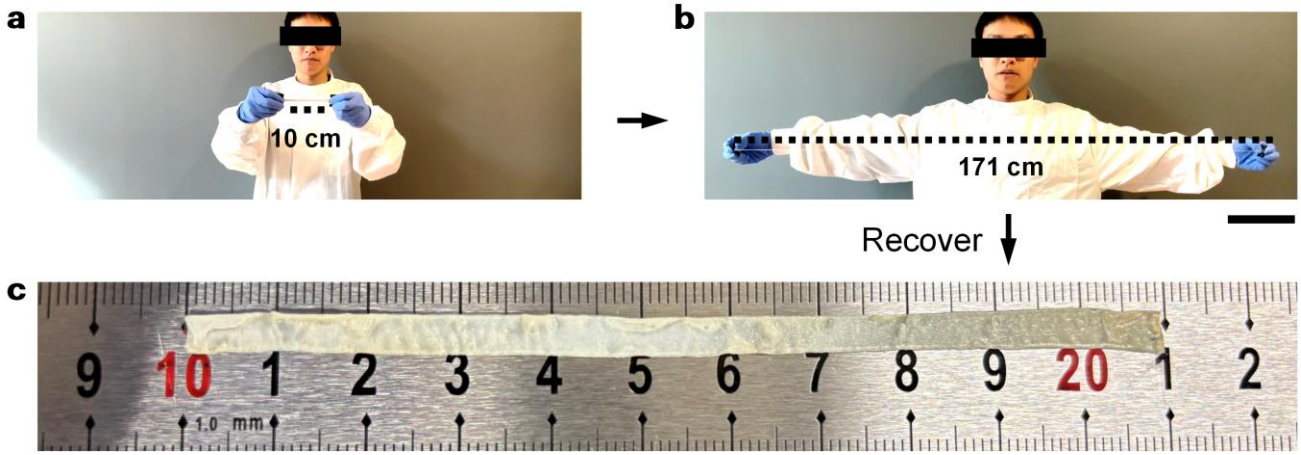

Supplementary Fig. S8. Arm-extension demonstration of LCE film (75% R-SH+1.0 wt% MXene). a, An initial LCE film with a length of 10 cm. **b**, The LCE film can be manually stretched to the length of an adult's fully extended arm (at least 171 cm). **c**, The stretched LCE film returned to approximately 11 cm after heating-induced nematic-isotropic transition. The scale bar is 20 cm. For the complete process, please refer to Supplementary Videos 2.

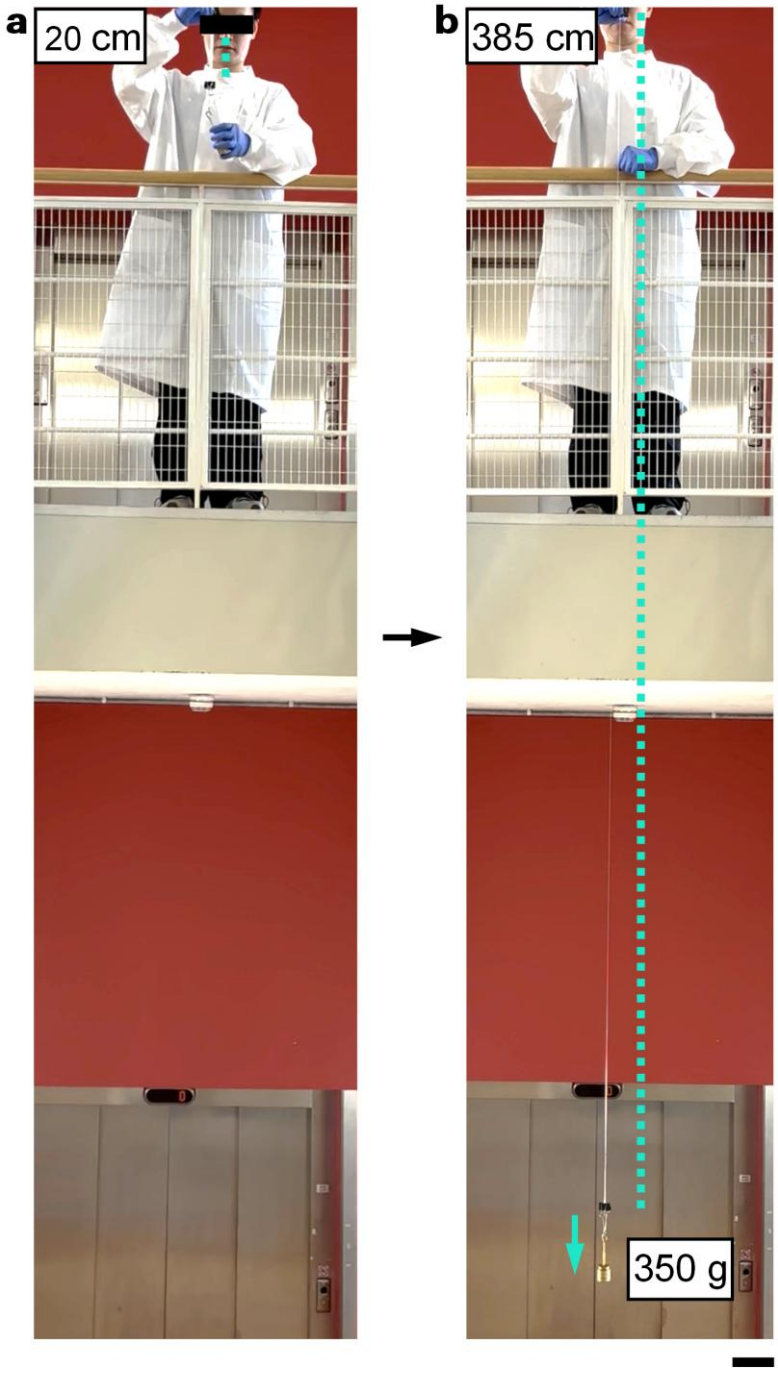

Supplementary Fig. S9. Ultimate drop stretch demonstration of the LCE film (75% R-SH+1.0 wt% MXene). a, An initial LCE film with a length of 20 cm. **b**, The LCE film can be stretched to at least 385 cm during the fall of a weight (350 g). The scale bar is 20 cm. For the complete process, please refer to Supplementary Videos 3.

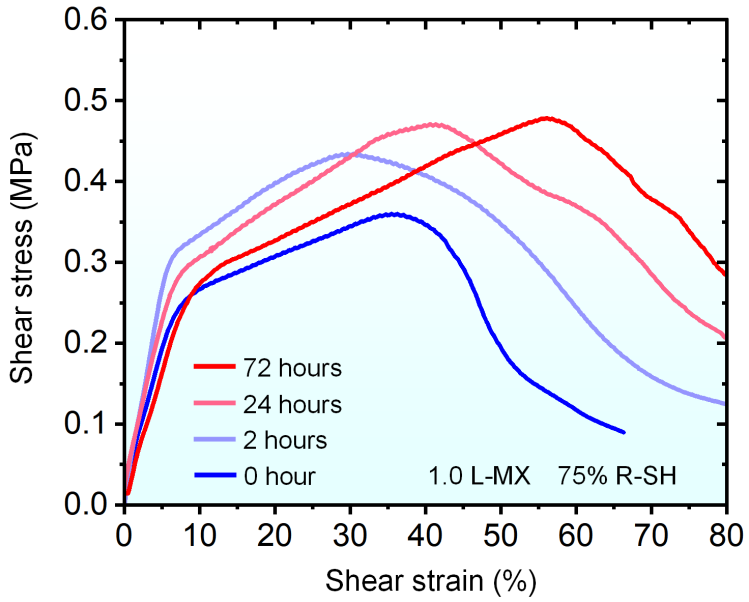

Supplementary Fig. S10. Lap shear strength for LCE film with different contact time. The lap shear strength of LCE film will increase as the contact time prolongs.

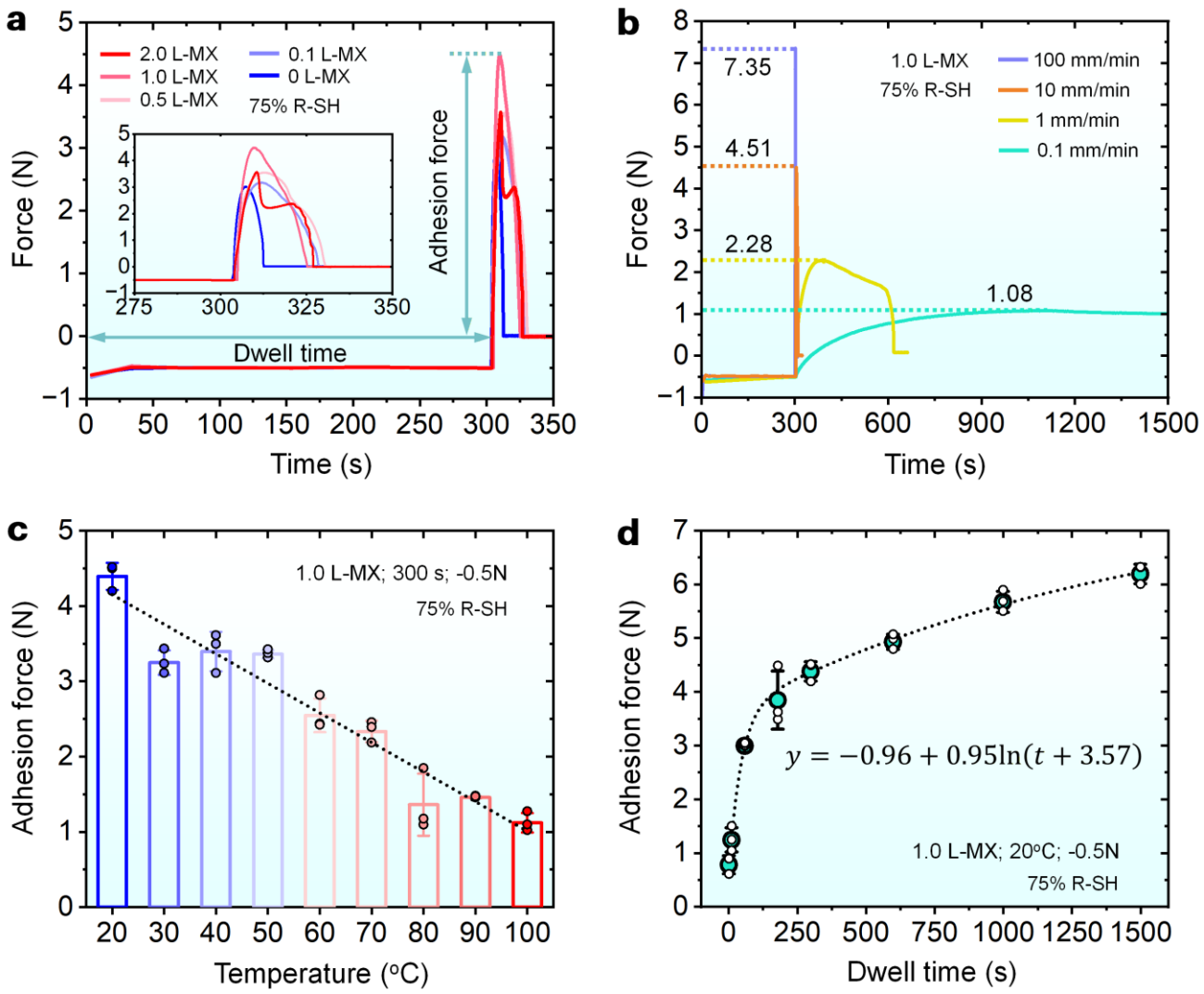

Supplementary Fig. S11. Probe-tack dynamic adhesion of LCE with MXene nanoplatelets. a, Dynamic adhesion curves of 75% R-SH LCE with different fraction of MXene nanoplatelets, at dwell time of 300 s and preload of −0.5 N. The embedding of MXene nanoplatelets enhanced the adhesion force of LCE, and the maximum adhesion was achieved when the mass fraction is 1 wt%. **b**, Dynamic adhesion of 1.0 L-MX with different pull-off velocity. Adhesion force will increase with the increase of pull-off velocity. The reduction in velocity will result in a longer duration for the process of the probe detaching from the LCE adhesion film (from 100 mm/min to 0.1 mm/min). This is attributed to the fact that the mesogens are more prone to undergo local rotation and reconfiguration at lower pull-off velocity, exhibiting better soft elasticity characteristics. **c**, Dynamic adhesion of 1.0 L-MX at different temperatures. The increase in temperature will lead to a nearly linear decrease in adhesion force, mainly due to the transition process of LCE from the nematic phase to the isotropic phase. **d**, Dynamic adhesion of 1.0 L-MX with different dwell time. The adhesion force exhibits a logarithmic growth trend over dwell time.

Supplementary Table S1. Comparison of the maximum adhesion strength and strain data presented in this work and the literatures.

References	Maximum adhesion strength (N/m)	Maximum strain (%)
Adv. Mater. **31**, 1902642 (2019)	17.3	120
ACS Appl. Mater. Inter. **12**, 31992-31997 (2020)	20	86
Ind. Eng. Chem. Res. **63**, 1432-1441 (2024)	70	326
Polymer **260**, 125377 (2022)	110	100
Small **18**, 2201012 (2022)	516	1164
J. Polym. Sci. Pol. Phys. **50**, 739-772 (2012)	550	27
Macromolecules **58**, 12191-12200 (2025)	638	490
ACS Appl. Mater. Inter. **16**, 6394-6402 (2024)	700	380
Macromolecules **56**, 6247-6255 (2023)	880	640
Adv. Mater. Technol. **11**, e00005 (2026)	900	150
Adv. Funct. Mater. **34**, 2309123 (2023)	1000	1200
Soft Matter **16**, 3267-3275 (2020)	1146	610
Adv. Mater. Inter. **11**, 2400448 (2024)	1300	450
Adv. Funct. Mater. **35**, e11426 (2025)	1451	567
Adv. Funct. Mater. **35**, 2413824 (2024)	1864	250
This work	**4687**	**1701**

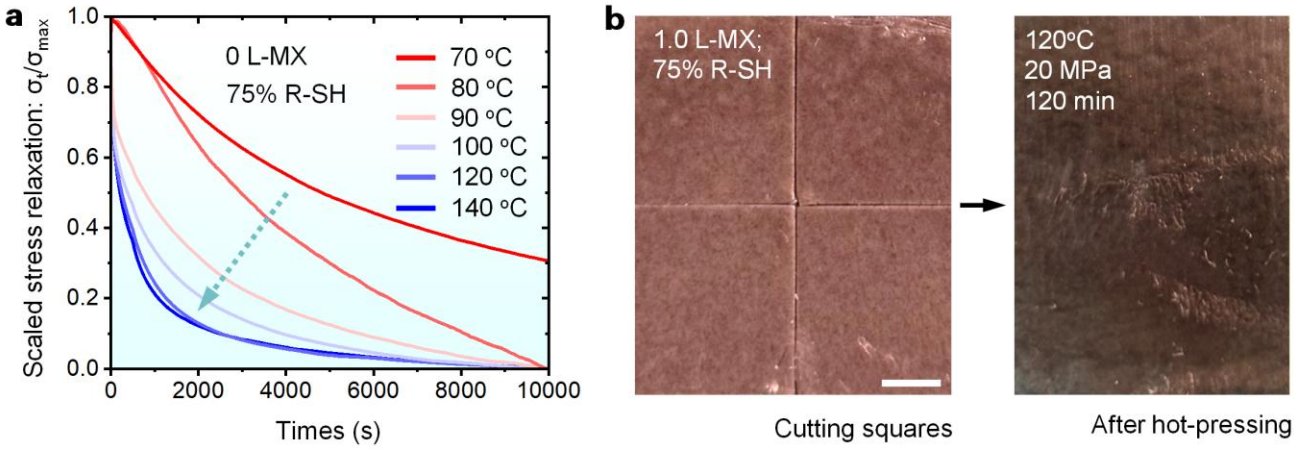

Supplementary Fig. S12. Dynamic adaptability of the LCE network. a, Stress relaxation curves of 0 L-MX at different temperatures. As expected, increasing the temperature will accelerate the stress relaxation process. **b**, An illustration of self-healing by hot-pressing of cutting pieces. The scale bar is 3 mm.

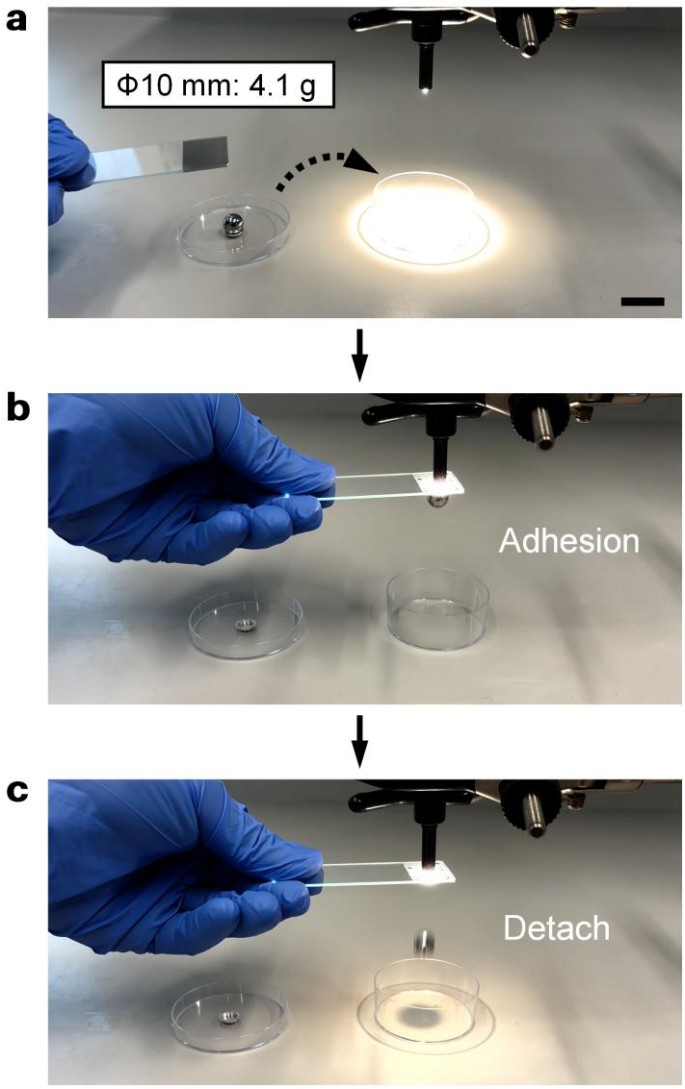

Supplementary Fig. S13. Demonstration of adsorption and transportation of 10 mm steel spherical object using LCE PSA. a, Adsorption process**. b,** Lifting and transportation process. **c,** Detachment process caused by illumination. The scale bar is 20 mm.

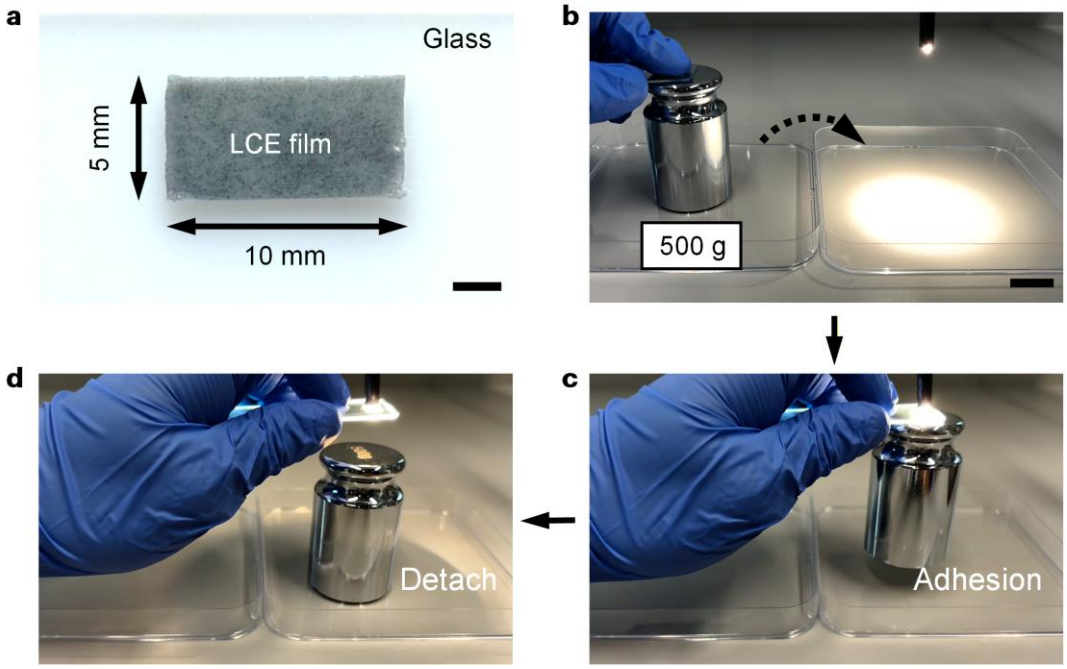

Supplementary Fig. S14. Demonstration of adsorption and transportation of 500 g stainless steel weight using LCE PSA. a, The photo of double-sided adsorbed LCE PAS. The scale bar is 2 mm. **b-d**, The adsorption, transfer and detachment processes of the weight using LCE PSA. The scale bar is 30 mm.

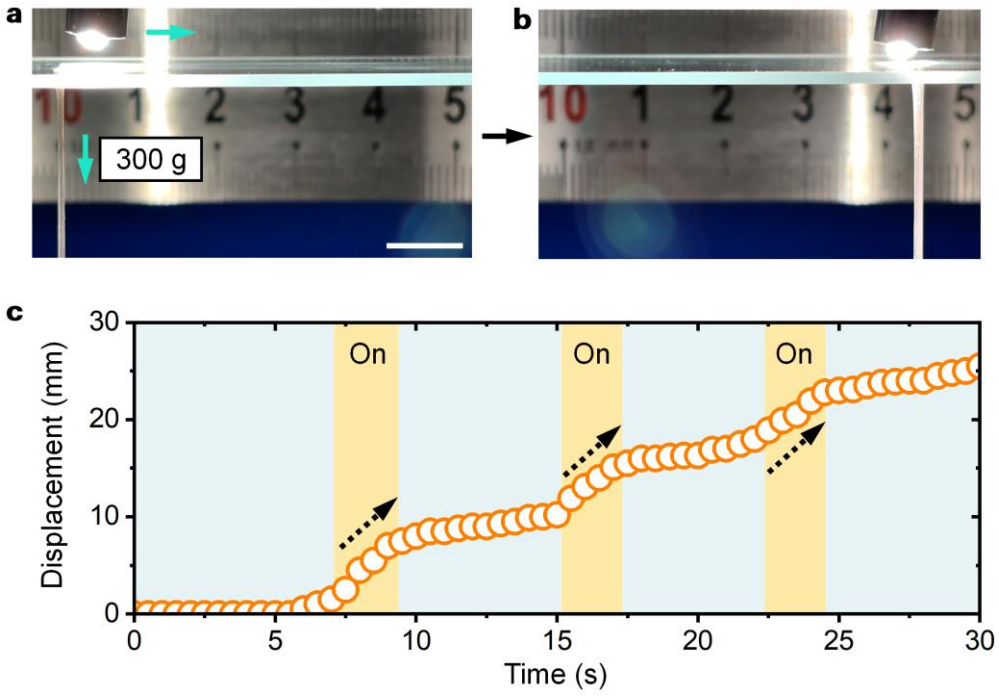

Supplementary Fig. S15. Demonstration of the light-controlled segmented 90°-peeling. (Supplementary Videos 9). a, The starting position for the light-controlled 90°-peeling test. **b**, The position where the 90°-peeling test was completed. **c**, The increase in peel displacement induced by illumination. The scale bar is 10 mm.

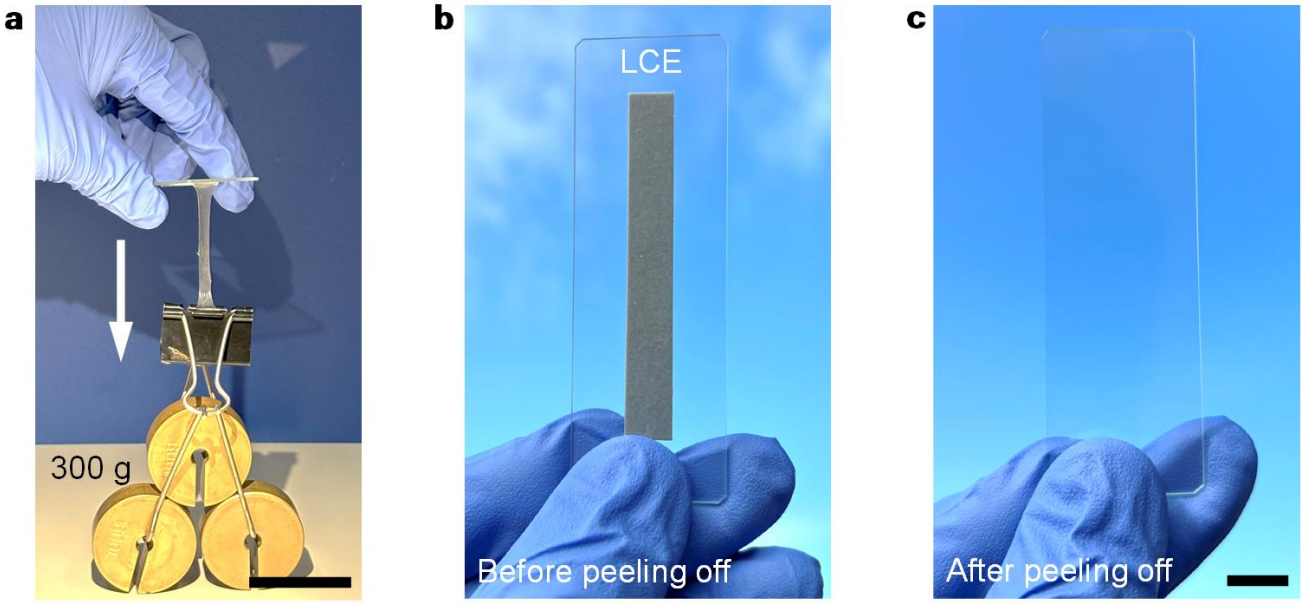

Supplementary Fig. S16. Photos of the weight and the glass substrate of the light-controlled segmented 90°-peeling. a, The image of hanging weight. The scale bar is 30 mm. **b**, The image of adsorbed LCE PSA film before peeling off. **c**, The image of clear glass surface after peeling off of LCE PSA film. The scale bar is 10 mm.